

## Crystallographic preferred orientation of bridgmanite: implications for the mantle dynamics in the lower mantle

Rheology is one of the most important physical properties of rock and minerals and plays a major role in controlling the dynamic processes in the Earth's mantle. The Earth's mantle consists of an upper mantle (depth: >410 km), transition zone (depth: 410–660 km) and lower mantle (depth: 660–2900 km), which have been distinguished by seismological and mineralogical studies. The lower mantle occupies ~65 vol% of the Earth's mantle. It is important for understanding the Earth's mantle dynamics to know the rheology of its lower mantle.

Recently, the results of P-wave tomography [1] have suggested four types of geometry of subducted slabs under the deep mantle; I-stagnant slabs above the 660 km discontinuity; II-slabs penetrating the 660 km discontinuity; III-slabs trapped in the uppermost lower mantle; and IV-slabs descending far into the deep lower mantle. Seismic tomography can be used to examine the present status of subducted slabs but does not give any direct insight into the flow directions of the slabs. On the other hand, seismic anisotropy, which could be caused by the crystallographic preferred orientation (CPO) of the constituent minerals yielded by deformation of the mantle dynamics, provides information on the flow direction in the deep mantle. At the uppermost part of the lower mantle around subduction slabs (e.g., the Tonga-Kermadec slab), seismic observation demonstrated clear shear wave splitting [2,3]. Therefore, if the CPO of the Earth's lower mantle minerals was well known, the observed seismic anisotropy could give insight into mantle flow directions around slabs.

In pyrolitic mantle model, the minerals constituting the lower mantle are bridgmanite (77 vol%), which is  $(\text{Mg,Fe})\text{SiO}_3$  perovskite with space group *Pbnm*, ferropericlaite (16 vol%) and  $\text{CaSiO}_3$ -perovskite (7%). The contribution to the CPO of ferropericlaite, which has nearly isotropic elasticity under the uppermost lower mantle conditions, is negligible.  $\text{CaSiO}_3$ -perovskite cannot contribute to seismic anisotropy in the lower mantle because of its very limited amount, although the elasticity of  $\text{CaSiO}_3$ -perovskite has large anisotropy. On the other hand, the seismic anisotropy is expected to be produced by the CPO of bridgmanite, which is an elastically anisotropic mineral and the most abundant mineral in the lower mantle. Thus, knowledge of the deformation-induced CPO of bridgmanite is the most important factor for understanding the mantle flow direction from the observed seismic anisotropy in the lower mantle.

The rheology of the lower mantle materials is unknown because of experimental limitations. The available maximum pressure and temperature for deformation experiments are still lower than the Earth's lower mantle conditions, although the experimental techniques at high pressures have significantly developed in the last decade (e.g., [4]). In this study, we further developed the experimental method for simple shear deformation experiments at high pressures to realize the deformation conditions (e.g., geometry and pressure) of the lower mantle using deformation-DIA-type high-pressure apparatus as a Kawai-type cell assembly (6–8 type). Shear deformation experiments on bridgmanite with a controlled strain rate under the uppermost lower mantle conditions (25 GPa and 1873 K) were performed for the first time using the developed techniques [5]. The starting materials were sintered  $(\text{Mg}_{0.97}\text{Fe}_{0.03})\text{SiO}_3$  bridgmanite aggregates, which had an equigranular texture with a typical grain size of 15  $\mu\text{m}$  and a random crystallographic orientation as shown in Fig. 1(a). Simple shear deformation of samples at a high pressure and high temperature was applied by 45°-cut alumina pistons and differential rams. The total strain and average strain rate of shear deformation under the uppermost lower mantle conditions were  $\gamma \sim 0.8$  and  $\dot{\gamma} \sim 2 \times 10^{-4}/\text{s}$ , respectively.

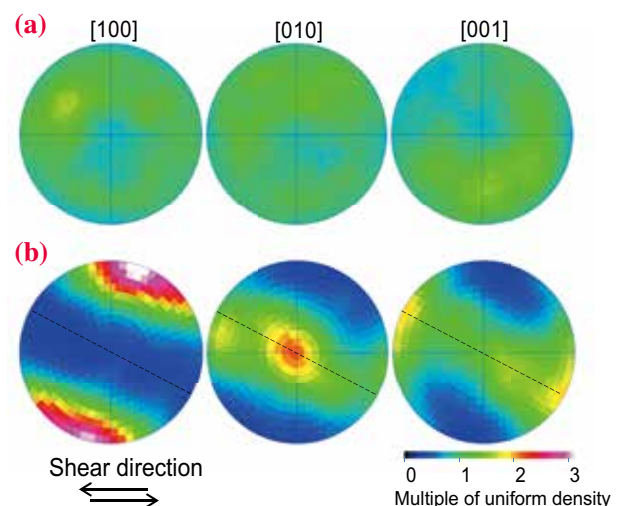


Fig. 1. Pole figures of bridgmanite showing the variation of the crystallographic orientation of the [100], [010] and [001] directions. The coordinate system is defined with respect to the deformation geometry of bridgmanite (a) before and (b) after shear deformation experiments. Black dashed lines represent the long axis of the strain ellipsoid of the deformed bridgmanite.

The crystallographic orientation of the bridgmanite before and after the shear deformation experiments was determined from the 2D monochromatic X-ray diffraction patterns collected at SPring-8 BL04B1.

Bridgmanite aggregates with shear deformation demonstrated a strong fabric (Fig. 1(b)), whereas the starting material had a random crystallographic orientation (Fig. 1(a)). In the sheared bridgmanite, the [001] direction is oriented parallel to the shear direction. The [100] and [010] directions are aligned perpendicular to the shear plane and normal to the shear direction on the shear plane, respectively. These results clearly indicate that the dominant slip system of bridgmanite is the [001](100) system under the conditions of 25 GPa and 1873 K, similar to the uppermost lower mantle conditions.

Figure 2 shows the shear wave anisotropy formed by the CPO of deformed bridgmanite in the present study, which was calculated on the basis of the elastic constant. Black dashes represent the polarization direction of the fastest shear wave in Fig. 2. For the shear wave anisotropy of deformed bridgmanite, in a horizontal flow, the velocity of horizontally polarized shear waves ( $V_{SH}$ ) is ~1% higher than that of vertically polarized shear waves ( $V_{SV}$ ), whereas  $V_{SV}$  is 0.03–1.10% higher than  $V_{SH}$  in a vertical flow. Figure 3 shows the observed shear wave splitting around the Tonga-Kermadec subduction slab, which is trapped at a depth of 1000 km in the uppermost lower mantle (type III according to P-wave tomography). Between the Tonga-Kermadec subduction zone and the Australian continental seismic station, shear wave splitting with  $V_{SH} > V_{SV}$  is observed above the subduction zone in the uppermost lower mantle. This seismic anisotropy can be explained by horizontal flow with the CPO of deformed bridgmanite, whose direction is parallel to

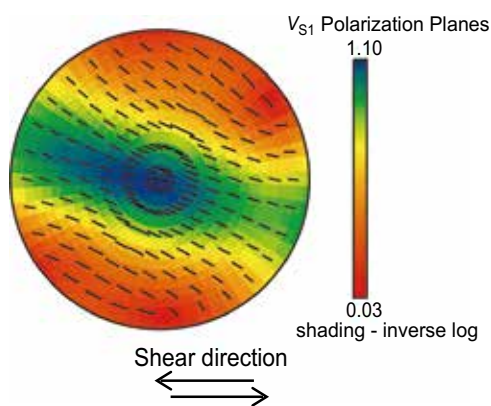


Fig. 2. Trace of the  $v_{S1}$  polarization plane of bridgmanite aggregates subjected to shear deformation under the uppermost lower mantle pressure and temperature in a horizontal flow.

the subducted plate. In addition, opposite shear-wave anisotropy ( $V_{SV} > V_{SH}$ ) was observed on the front arc side from the Tonga-Kermadec subduction zone to the western North America stations. To explain the seismic anisotropy, a vertical flow is needed with the CPO of deformed bridgmanite. It is thus concluded that both the observed shear-wave anisotropies around the Tonga-Kermadec subduction zone are well explained by the CPO of bridgmanite yielded by the penetration of subducted slabs down to 1000 km by vertical motion and by the stagnation at around 1000km depth with a horizontal flow in the pyrolitic mantle as shown in Fig. 3. Therefore, the present results on CPO of the bridgmanite coupled with the observation of seismic anisotropy provide strong evidence for understanding the direction of the mantle flow, which can be predicted from seismic tomography.

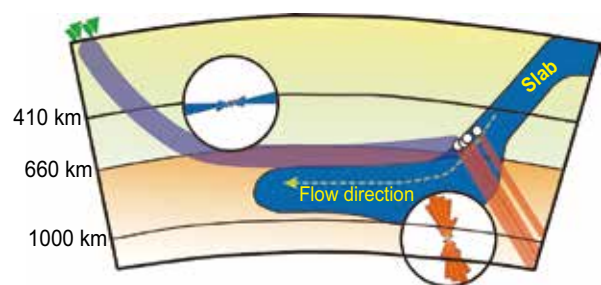


Fig. 3. Schematic cross section of subducted slab of the Tonga-Kermadec arc. Blue and orange lines respectively represent shear seismic ray paths nearly parallel and perpendicular to the section used for the observation of shear wave anisotropies. Blue and orange polar histograms show the polarization of the fast shear wave perpendicular to blue and orange seismic ray paths, respectively. Yellow dashed lines correspond to flow direction of the subducted slab.

Noriyoshi Tsujino<sup>a,\*</sup>, Yu Nishihara<sup>b</sup> and Daisuke Yamazaki<sup>a</sup>

<sup>a</sup>Institute for Planetary Materials, Okayama University

<sup>b</sup>Geodynamics Research Center, Ehime University

\*Email: tsujino@okayama-u.ac.jp

## References

- [1] Y. Fukao & M. Obayashi: J. Geophys. Res. **118** (2013) 5920.
- [2] J. Woocky *et al.*: Nature **415** (2002) 777.
- [3] A. Nawacki *et al.*: Geochem. Geophys. Geosys. **16** (2015) 764.
- [4] T. Kawazoe *et al.*: American Mineral. **96** (2011) 1665.
- [5] N. Tsujino, Y. Nishihara, D. Yamazaki, Y. Seto, Y. Higo, E. Takahashi: Nature **539** (2016) 81.